Applied Thermal Engineering 29 (2009) 1398–1405

Contents lists available at ScienceDirect

Applied Thermal Engineering

journal homepage: www.elsevier.com/locate/apthermeng

Comparison of measured and modelled droplet–hot wall interactions

D. Chatzikyriakou [a,*], S.P. Walker [a], G.F. Hewitt [b], C. Narayanan [c], D. Lakehal [c]

[a] Department of Mechanical Engineering, Imperial College London, Exhibition Road, London SW7 2AZ, UK
[b] Department of Chemical Engineering and Chemical Technology, Imperial College, Prince Consort Road, London SW7 2BY, UK
[c] ASCOMP GmbH, Technoparkstrasse 1, 8005 Zurich, Switzerland

ARTICLE INFO

Article history:
Received 16 December 2007
Accepted 12 February 2008
Available online 20 February 2008

Keywords:
Droplet
Leidenfrost
Vapour layer
Level Set

ABSTRACT

In this study CFD simulations of both sessile droplets resting upon a vapour cushion and droplets bouncing off a hot solid surface are presented. As a droplet approaches a hot surface the vapour layer formed by evaporation from the droplet acts like a cushion and can prevent contact between the liquid and the hot surface. Rather than hitting and wetting the surface, the droplet can rebound from the vapour film. For the tracking of the interface between the two fluids a one-fluid Level Set method is used, embodied in the TransAT© finite-volume two-phase flow computational code. Inter alia, this incorporates a full Navier–Stokes solution in the region of the thin film. The method is used to analyse the experiments conducted by Wachters et al. [L.H.J. Wachters, H. Bonne, H.J. Van Nouhuis, The heat transfer from a horizontal plate to sessile water drops in the spheroidal state, Chemical Engineering Science 21 (1966) 923–936] and Biance et al. [A.-L. Biance, F. Checy, C. Clanet, G. Lagubeau, D. Quere, On the elasticity of an inertial liquid shock, Journal of Fluid Mechanics 554 (2006) 47–66]. Good agreement with the experimental observations is obtained.

1. Introduction

The phenomenon of the impingement of liquid droplets onto superheated surfaces is of great importance in many industrial applications. One occasion when the cooling of a hot surface by impingement of water droplets is important is the recovery process (“reflood”) following a postulated Loss-of-Coolant-Accident (LOCA) in a Pressurised Water Nuclear Reactor (PWR). Following a LOCA, the fuel elements rise rapidly in temperature, reaching typically 600–900 °C. Water is then introduced into the bottom of the reactor vessel (“bottom reflooding”) from the Emergency Core Cooling System (ECCS). A two-phase mixture rises up around the fuel rods. During this process a rewetting front is formed at the bottom of the fuel elements and this front slowly rises up the fuel element. Above the rewetting front, liquid is present in the form of a liquid core, swept upwards by the vapour flow, which breaks up in a complex way to form drops. Cooling of the fuel by this droplet–steam mixture above the rewetting front (“precursory cooling”) is vitally important in the reflood process. In this region the conditions are characterized by flow of superheated vapour between even hotter metal surfaces, with a population of small saturated droplets entrained in the vapour flow. It is important to understand the mechanisms by which droplets interact with hot surfaces, and this is the focus of the work described here. Ultimately, with this and subsequent studies, we would like to be able to answer questions along the lines of “Just how much heat is removed from a hot metal surface by the non-wetting bouncing of a droplet?”

When a droplet impacts upon a hot solid surface, heat is transferred from the solid to the liquid and vapour phases. This both increases its mean temperature (if it is subcooled) and evaporates liquid from the droplet. If the heat transfer rate is large enough during the impact, liquid vapourized from the droplet forms a vapour layer between the liquid and the solid surface, preventing direct contact of the droplet with the surface. In this case, heat transfer is reduced and the ‘evaporation lifetime’ of the droplet is increased. This phenomenon was first observed by Leidenfrost [1] and therefore this behaviour is known as the Leidenfrost phenomenon.

In order to characterize the behaviour of the droplets under such circumstances, information such as the momentum change, and understanding of the heat transfer between the droplet and the solid surface and the residence time of the droplet needs to be gained, either experimentally or computationally. The processes following the interaction of a droplet on a hot surface (spreading, recoiling, bouncing and evaporating) are complicated, and depend on a number of parameters such as the droplet and the surface temperature, the droplet size, the surface roughness and the droplet impact velocity.

Modern CFD techniques offer the ability to model two-phase flow accounting explicitly for exchanges in mass, momentum and

* Corresponding author.
E-mail address: d.chatzikyriakou@imperial.ac.uk (D. Chatzikyriakou).

1359-4311/$ - see front matter © 2008 Elsevier Ltd. All rights reserved.
doi:10.1016/j.applthermaleng.2008.02.012

Nomenclature

Latin symbols

d	re-distance function
$\tilde{D}$	viscous stresses tensor (1/s)
g	gravity (m/s^2)
H	smoothed Heaviside function
$\dot{m}''$	interface mass transfer rate per unit area (kg/m^2 s)
p	pressure (Pa)
R	droplet radius (m)
$\vec{V}$	velocity vector (m/s)
Re	Reynolds number
We	Weber number

Greek symbols

δ	Dirac delta function
ε	thickness of interface
κ	surface curvature (1/m)
μ	absolute viscosity (kg/m s)
ρ	density (kg/m^3)
σ	surface tension coefficient (N/m)
τ	pseudo time (s)
ϕ	Level Set function

Subscripts/superscripts

int	interface
g	gas
l	liquid
k	$k = 1$ for gas and $k = 2$ for liquid

energy between the phases. In this study we attempt, with CFD modeling, to examine the interaction of droplets with hot solid surfaces, and in particular we attempt to reproduce the results of earlier experimental measurements and associated analytical modelling. In the following section a review of previous experimental and computational work in this field is presented. In Section 3, the computational model and schemes used for this study are described. Then, in Section 4, the phenomenon of a water droplet resting on a hot (beyond-Leidenfrost) wall is studied by reproduction of an experiment conducted by Wachters et al. [2]. Then, moving on to the dynamic part of the phenomenon, a water droplet impacting on a beyond-Leidenfrost temperature wall is examined and the results are compared with previous experimental data and analytical correlations of Biance et al. [3]. Finally, concluding remarks summarize the work presented here and provide an overview of the results obtained.

2. Previous studies

2.1. Previous experimental studies

Experiments observing the behaviour of droplets when they impinge on a very hot (beyond-Leidenfrost), dry wall have indicated the multi-parametric nature of this phenomenon. A criterion to categorize interactions is the 'impacting' velocity of the droplet. Depending on its value, one can divide these into sessile droplet and impacting droplet cases, respectively.

Wachters [2] and Wachters and Westerling [4] performed extensive studies on the influence of the solid surface temperature on droplet impact. A critical temperature was found above which droplet rebound is observed. More specifically, Wachters [2] observed that for sessile water droplets in dry air environment this temperature would exceed 220 °C and the droplets would be sustained above the hot surface retaining a spheroidal state. Biance et al. [5] who studied sessile droplets showed that for very small droplet sizes, that part of the droplet in close proximity to the hot surface plays a minor role in the evaporation process, since its surface area vanishes rapidly as the droplet diameter reduces.

Pedersen [6] focused on experimental studies concerning the velocity of the droplet and how this affects the subsequent interaction. He identified a minimum velocity below which the droplet deforms considerably without break-up upon impingement. Okumura et al. [7] showed that spreading of the droplet during the interaction with the wall increases with velocity. Biance et al. [3], both with analytical and experimental studies, agreed with this observation. They showed that there is a direct dependence of the base radius on the Weber number (for a given fluid this indicates dependence on the velocity). They proposed an analytical model describing this dependence, and obtained experimental results in accordance with it.

2.2. Previous computational studies

A major part of previous computational studies was concerned with the impact of droplets on the surface, the spreading and the recoiling of the droplet and the deformation process. In other words, the main emphasis has been given to the hydrodynamic part of the phenomenon. The evaporation process during the impact was normally neglected. The main difference between the computational approaches lies in the numerical methods used to simulate this two-phase flow phenomenon and the different models created to simplify this complex analysis. Starting from very early attempts to capture the constantly deforming interface between the two phases, various computational algorithms have been developed. The most recent and most widely used ones are the Volume of Fluid (VOF) and the Level Set (LS) methods.

Very early attempts, such as that of Harlow and Shannon [8] employed the MAC (Marker And Cell) method in order to simulate the droplet–solid surface interaction. However, in their study, the viscosity and the surface tension forces in the momentum conservation equations were ignored. A volume-tracking methodology was used by Bussman et al. [9,10]. They developed a three-dimensional model based on the RIPPLE code [11] to simulate the droplet collision and splash on an inclined surface. The effect of surface tension was taken into account by the Continuum Surface Force (CSF) model [12]. This model was later applied to analyze the splash of a droplet impacting onto a solid [10]. In a later study, Pasandideh-Fard et al. [13] solved the momentum and heat transfer equations that describe the droplet deposition on the solid substrate, by using a modified-VOF method. Additionally, Pasandideh-Fard et al. [14] extended Bussmann's [9,10] model by including the effects of heat transfer and solidification of liquid drops.

Wu et al. [15] simulated the formation, ejection, and impact of a liquid droplet in an inkjet device by the VOF and CSF techniques. Fukai et al. [16] used the adaptive-grid finite element method to simulate the droplet impact. Fukai et al. [17] also considered the wettability of the solid surface on the contact line between liquid and solid, as the droplet is spreading and receding. Perot and Nallapati [18] utilized a moving unstructured staggered mesh method to study the collision of droplets onto a solid. Baer et al. [19] proposed a model for analyzing free surface flows by employing a

Finite Element Method (FEM). The motion of a droplet down an inclined plane was simulated. Theodorakakos and Bergeles [20] developed a model that combined the VOF method and the adaptive-grid refinement method to simulate the impact of a small drop onto a solid surface. Francois and Shyy [21] used the Immerse Boundary method (IB) to study the effect of different *We* and *Re* numbers on the droplet impact phenomenon. Numerical studies on the collision of liquid droplets with a solid surface have been performed by Hatta et al. [22], Fujimoto and Hatta [23] and Fujimoto et al. [24,25] who used the VOF technique to track the free liquid surface. Normal and oblique collisions of droplets with the substrate were simulated at low droplet impact inertia. The influence of impact angle was examined and the experimental observations and the numerical results were in reasonable agreement. Recently, Caviezel et al. [26] investigated moderate Reynolds number droplet flows, for which two-dimensional axisymmetric simulations using the TransAT© code [27,28] which is employing the Level Set method, were performed. A drop-impact regime map was generated. In that map the impact dynamics were characterized as a function of Weber number and equilibrium contact angle.

Numerical approaches for the beyond-Leidenfrost regime have employed mostly the VOF and the Level Set method (LS). Karl et al. [29] used the VOF method in order to simulate tiny droplet interactions with hot walls, with surface temperatures exceeding the Leidenfrost condition. To reproduce the phenomenon in a more realistic way, they applied a free-slip boundary condition and a contact angle of 180° on the solid surface. The no-slip condition was applied in the spreading phase and the free-slip condition was used in the recoiling stage in the simulations by Fujimoto and Hatta [23], who used a two-dimensional MAC-type method. The effects of the evaporation and the vapour flow were neglected and a simplified temperature field was assumed. The VOF method was used by Harvie and Fletcher [30,31], who developed an axisymmetric, 2D algorithm in order to simulate the volatile liquid droplet impacting on a hot solid surface. They described the vapour flow between the droplet and the solid surface by a 1D flow model. Their model neglects the inertial force of the flow but could predict the droplet dynamics accurately for *We* number below 30. Ge and Fan [32] carried out a three-dimensional simulation of a droplet impacting onto a hot flat surface in the Leidenfrost regime. The Level Set method in a finite-volume algorithm with the Arbitrary Lagrangian–Eulerian (ALE) technique was adopted. In a later work, Ge and Fan [33] considered also the heat transfer both inside each phase and at the solid–vapour/liquid–vapour interface in their model. The vapour flow dynamics and the heat flux across the vapour layer were solved with consideration of the kinetic discontinuity at the liquid–vapour and solid–vapour boundaries in the slip-flow regime. They employed the same model that Harvie and Fletcher [30,31] had used for the modeling of the vapour layer between the droplet and the solid surface. Additionally, Ge and Fan [32,33] have shown good agreement between their simulated results and experimental results of Chen and Hsu [34], concerning the temperature drop and consequently the heat transfer inside the solid surface.

We here will build upon these earlier works, by using a finite-volume Level Set approach that embodies a full (Navier–Stokes) solution for the vapour flow beneath the droplet (and of course elsewhere), with this vapour flow mechanistically coupled to the vapour mass efflux from the droplet surface.

3. Computational model

3.1. Physical model

In the present computational work, the dynamic interaction of a droplet with a hot substrate is simulated. For the dimensions and velocities studied, the whole flow field, both in the drop and in the surrounding vapour, is laminar. In the present version, evaporative mass transfer from the droplet to the vapour is approximated by specifying a uniform mass transfer rate per unit droplet surface area. The energy equation is not solved; heat transfer within the droplet or vapour is not modelled. The micro-flow under the droplet lower surface is, like the whole flow field, studied by 'exact' solution of the flow equations; no empirical 'vapour layer model' is used. The droplet is assumed to be spherical at the beginning of the simulation and the fluids comprising the computational domain (liquid and gas) are treated as incompressible and immiscible. Water and water vapour comprise the two phases present.

3.2. Numerical method

3.2.1. TransAT© code

We employ the CMFD code TransAT© developed at ASCOMP. This is a multi-physics, finite-volume code based on solving multifluid Navier–Stokes equations. The code uses structured meshes, though it allows for multiple blocks to be set together. The grid arrangement is collocated. The solver is pressure based (projection type), corrected using the Karki–Patankar technique for compressible flows (up to transonic flows). High-order time marching and convection schemes can be employed, and up to third-order monotone schemes in space. Multiphase flows are tackled using interface tracking techniques for both laminar and turbulent flows. The one-fluid formulation context on which TransAT© is built is such that the two-phase flow is represented as the flow of one-fluid having physical properties which vary according to a "color function" as it is advected by the flow. This allows identification of the local phase (gas or liquid). Either the Level Set or the Volume-of-Fluid Interface Tracking Methods (ITM) can be employed in the code to track evolving interfaces. In the present work, the Level Set method was employed.

3.2.2. Droplet surface tracking method

Capturing the interface between the droplet and the surrounding gas involves the use of an interface tracking method appropriate for fixed Eulerian grids. Here, the Level Set method, introduced by Osher and Sethian [35], is being employed. The main advantage of this method is the inherent ability to handle topological changes in a straightforward way. It has been proved to be very reliable in the simulation of curvature-dependent problems such as interface breaking and merging.

Here, the Level Set function ϕ is used in order to separate the liquid and the gaseous phases. The free surface of the droplet is designated by the set of points where $\phi = 0$. Generally, in the computational domain, the Level Set function is defined as follows:

$$\begin{aligned} &\phi(\vec{x},t) > 0 \quad \text{for } \vec{x} \text{ in the liquid phase} \\ &\phi(\vec{x},t) < 0 \quad \text{for } \vec{x} \text{ in the gas phase} \\ &\phi(\vec{x},t) = 0 \quad \text{for } \vec{x} \text{ at the interface} \end{aligned} \tag{1}$$

The motion of the interface moving with velocity $\vec{V}^{\text{int}}$ is captured by evolving the Level Set equation (a Hamilton–Jacobi type convection equation) in the computational domain

$$\frac{\mathrm{d}\phi}{\mathrm{d}t} + \vec{V}^{\text{int}} \cdot \nabla\phi = 0 \tag{2}$$

The entire computational domain can be treated as a single domain and the regions of different materials can be distinguished using the Level Set function. The density and the viscosity of the whole fluid change continuously from one phase to the other and are defined as

$$\rho(\phi) = \rho_g + (\rho_l - \rho_g)H(\phi) \quad (3)$$

$$\mu(\phi) = \mu_g + (\mu_l - \mu_g)H(\phi) \quad (4)$$

where the subscripts l and g denote the liquid and the gas phase, respectively and $H(\phi)$ is a (smoothed) Heaviside function defined as follows (where ε is the interface thickness):

$$H(\phi) = \begin{cases} 0 & \text{if } \phi < -\varepsilon \\ \frac{1}{2}\left[1 + \frac{\phi}{\varepsilon} + \frac{1}{\pi}\sin\left(\pi\frac{\phi}{\varepsilon}\right)\right] & \text{if } |\phi| \leqslant \varepsilon \\ 1 & \text{if } \phi > \varepsilon \end{cases} \quad (5)$$

Numerical diffusion causes the interface to smear around the interface after a single advection stage, which in practice means that the Level Set ceases reliably to indicate the phase of the fluid. To restore the correct behaviour near the interface an iterative re-distancing procedure is performed. During this process the Level Set function ϕ is set to be equal to a distance function d that is defined as the signed distance function from a given point in the computational domain to the interface between the two phases. In that context, the following equation (Eq. (6)) has to be integrated to steady state [36]:

$$\frac{\partial d}{\partial \tau} - \mathrm{sgn}(d_o)(1 - |\nabla d|) = 0$$
$$d_o(\vec{x}, \tau = 0) = \phi(\vec{x}, t) \quad (6)$$

The re-distance function 'd' is nothing else than the Level Set function ϕ itself at the previous time step.

$$d(\vec{x}, t) = \phi(\vec{x}, t - \Delta t) \quad (7)$$

Eq. (6) is solved after each advection step of Eq. (2), using the non-oscillatory third-order WENO (Weighted Essentially Non-Oscillatory) scheme.

3.2.3. Hydrodynamic model

The incompressible Navier–Stokes equations. The equations for viscous incompressible flows that describe the conservation of mass and momentum in a Cartesian coordinate system are

$$\nabla \vec{V} = 0 \quad (8)$$

$$\rho\left(\frac{\partial \vec{V}}{\partial t} + \nabla \cdot \vec{V}\vec{V}\right) = -\nabla p + \rho\vec{g} + \nabla \cdot (2\mu\tilde{D}) + \sigma\kappa(\phi)\delta(\phi)\nabla\phi \quad (9)$$

where $\vec{V}$ is the fluid velocity, p is the pressure, ρ is the density as derived in Eq. (3), μ is the fluid viscosity as derived in Eq. (4), $\tilde{D}$ is the viscous stresses tensor, σ is the surface tension coefficient, $\delta(\phi)$ is the one-dimensional Dirac delta function, and $\kappa(\phi)$ is the curvature of the free surface calculated by means of the Level Set function ϕ:

$$\kappa(\phi) = \nabla \cdot \frac{\nabla\phi}{|\nabla\phi|} \quad (10)$$

The last term in Eq. (9) represents the surface tension force and is incorporated in the computational modeling as a force that acts only on the computational cells in the vicinity of the free surface. Here, this vicinity is assigned the thickness ε.

The third-order QUICK scheme is employed to calculate the convective terms of both the Navier–Stokes transport equations and the Level Set equation and a third-order Runge–Kutta method is used for the advancing of the time step. Adaptive time-stepping is used choosing the overall time step based on convection, viscosity, surface tension and gravity.

3.2.4. Heat/mass transfer model

The current TransAT© version includes correlations for the modeling of heat transfer between the interface and the bulk fluids on either side of it. It does not describe the heat transfer across the interface leading to evaporation of the liquid to form vapour in the interface region. Therefore, the heat transfer from the vapour to the liquid phase is introduced to the model as a mass transfer term through the interface between the gas and the liquid. This mass flux (evaporation) is associated with phase change in the computational model used and the necessary jump conditions are

$$\sum_{k=1}^{2} \dot{m}_k'' = 0 \quad (11)$$

$$\dot{m}_k'' = \rho_k(V_j^k - V_j^{\mathrm{int}}) \cdot n^k \quad (12)$$

Here $\dot{m}_k''$ is the interface mass transfer rate per unit area, V_j^{int} and V_j^k are the front and the flow field velocity components, respectively. The subscript k denotes the phase to which we refer to; that is $k = 1$ for the vapour phase and $k = 2$ for the liquid phase. n^k is the vector normal to the interface defined as:

$$n^k = -\frac{\nabla\phi}{\|\nabla\phi\|} \quad (13)$$

Given the continuity jump condition and using that $n^1 = -n^2$, the mass flux from any of the two phases towards the other is expressed by means of Eq. (12).

The component of the velocity of the interface V^{int} normal to the interface direction is expressed as follows, taking into account Eq. (12):

$$V^{\mathrm{int}} = V_j^{\mathrm{int}} \cdot n^k = V_j^k \cdot n^k - \frac{\dot{m}_k''}{\rho_k} \quad (14)$$

The interface mass transfer rate, $\dot{m}_k''(\mathrm{kg/m^2 s})$, is prescribed and remains constant through time over the whole droplet surface.

3.3. Droplet modelling issues

All simulations here employ an axisymmetric two-dimensional fixed Cartesian grid with non-uniform grid spacing. The grid is refined in the regions of greatest interest; the droplet and the vapour layer below the droplet. The grid spacing in those regions is of the order of 0.04 mm. The water droplet radius is 0.89 mm and 1 mm, respectively for the two separate cases simulated, with 44 and 50 grid points per diameter, respectively. The average time step is around 1.5 μs.

The model described is used to simulate a millimetric water droplet impinging on a surface without initial velocity (sessile) and with initial velocity. The case of the millimetric droplet without phase change (i.e. no prescribed mass efflux from the droplet surface) is also simulated to serve as a comparison with the evaporating sessile droplet case.

4. Results and discussion

4.1. Introduction

We will now address two main cases; those of a 'sessile' and an 'impacting', droplet. In the first, a droplet is released in very close proximity to a surface with zero initial velocity and in the second it approaches with significant momentum. For the second case the deformation of the droplet is examined initially, and then a quantitative assessment is made of the maximum base radius attained.

The sessile case allows us to make comparisons of the equilibrium vapour film thickness with similar 'sessile' measurements of Wachters et al. [2], providing a valuable opportunity for validation of the computational approach.

This allows extension with confidence to the more demanding case of the impacting drop. Here we will make comparison of computed droplet behaviour both with the experimental photographic record of droplet shape, and with the experimental and analytical correlations of droplet size during the spreading phase [3].

4.2. Sessile droplet case

4.2.1. Experiment

Wachters et al. [2] observed experimentally the phenomenon of small droplets (known as sessile droplets) 'resting' on a beyond-Leidenfrost temperature wall. A known amount of water was placed upon a concave hot plate of polished gold. This plate was heated by means of an electrical heater. The temperature of the hot plate was measured by means of a thermocouple mounted on it. After allowing enough time for the oscillations of the droplet to die out, the droplet and part of the hot plate were photographed from the side.

From the photographs, Wachters et al. [2] obtained the rate of change of volume and the volume of the droplet as functions of time. This allowed them to assess the evaporation rate of the sessile droplet as well as the thickness of the vapour layer formed below the droplet sustaining it. They also observed that once the droplet comes to a balance and its lower surface has become slightly flattened, the evaporation rate at the bottom of the droplet becomes uniform. At the same time, the droplet evaporates from the sides with a slightly higher evaporation rate. These measurements agreed with a simple theory presented by the same researchers. The aforementioned considerations have led us to investigate whether the phenomenon of a tiny sessile droplet balancing on a vapour layer and evaporating can be reproduced in a reasonably realistic way by the prescription of a uniform evaporation rate.

Wachters et al. [2] conducted this experiment for a series of droplet sizes and a series of wall temperatures. The one of interest to us was the case of a 0.89 mm radius droplet resting on a 400 °C surface. It was reported that the vapour layer thickness sustaining the droplet acquired a value of 28.9 μm after the droplet had stopped oscillating. In this state, the overall evaporation rate of the droplet was found to be uniform in time and equal to 0.151 mm^3/s.

4.2.2. Computational simulation

We have used the models outlined above to simulate the aforementioned experiment. The properties of the fluids were: The density ratio between the two phases was $\rho_l/\rho_g = 1662$ and the viscosity ratio was $\mu_l/\mu_g = 280$. The surface tension coefficient was 0.058 N/m (water at 100 °C). An issue in our study was the definition of the initial droplet position, and the shape of the droplet when evaporation starts taking place. In reality, as reported by Wachters et al. [2], the droplet acquires a fairly flat bottom surface almost immediately after coming into close proximity with the hot wall. The experimental measurements provide the equilibrium rate of vapour generation and the equilibrium height of the droplet above the surface (but not the droplet shape). As noted, at present the code used has only the capability to specify the rate of generation of vapour, rather than compute it mechanistically. In order to model the particular experimental case, the droplet is released (as a sphere) from an initial height 50 μm above a solid surface. The vapour generation rate is then adjusted manually until the droplet reaches an equilibrium shape at the experimentally observed height. One indication of the goodness of the simulation is then given by near equality of the computational vapour generation rate required to achieve this (0.150 mm^3/s) with the experimental vapour generation value (0.151 mm^3/s).

Then, the same 0.89 mm radius water droplet was released, again with zero velocity 50 μm above the solid surface, but this time without any evaporation taking place. This case was simulated to serve as a comparison between the evaporating and the non-evaporating regimes in terms of droplet shape and wetting of the hot surface.

In our simulation, the evaporating droplet is sustained by a vapour layer as observed in the experiment. The same droplet, when released at the same height with no evaporation, simply rests upon the surface, as would be expected. Fig. 1 shows snapshots of the droplet shapes and positions in the two cases at a series of times.

Fig. 2 shows the variation through time of the vapour layer thickness beneath the droplet centre. As is seen, after about 7 ms, the film thickness takes on a value oscillating around about 30 μm. This is achieved with a vapour generation rate of 0.150 mm^3/s. The corresponding experimental values were 28.9 μm and 0.151 mm^3/s, respectively, indicating very good agreement.

This provides good validation of the model adopted in this study. The mass transfer rate model used here, which applies a spatially and temporally uniform rate of vapour generation over the entire droplet surface, can satisfactorily reproduce the experimentally observed behaviour of a millimetric water droplet resting on a beyond-Leidenfrost temperature solid, dry wall. Whilst a more mechanistic model would of course compute the local vapourisation

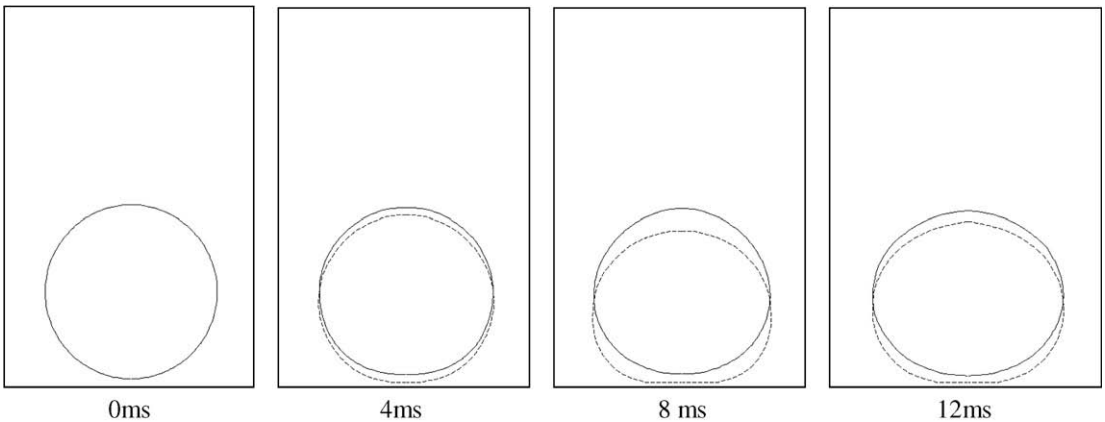

Fig. 1. Two-dimensional axisymmetric case of droplet left with zero velocity just above a solid surface. Solid line: Case where a 0.89 mm radius water droplet evaporates and the hot solid surface is sustained at 400 °C. A vapour cushion can be observed below the droplet. Dashed line: A 0.89 mm radius droplet is left above a solid surface sustained at the same temperature with the droplet. No evaporation is present and the droplet slowly impacts on the solid surface. The whole computational domain is not presented here to allow better visualization of the region of interest.

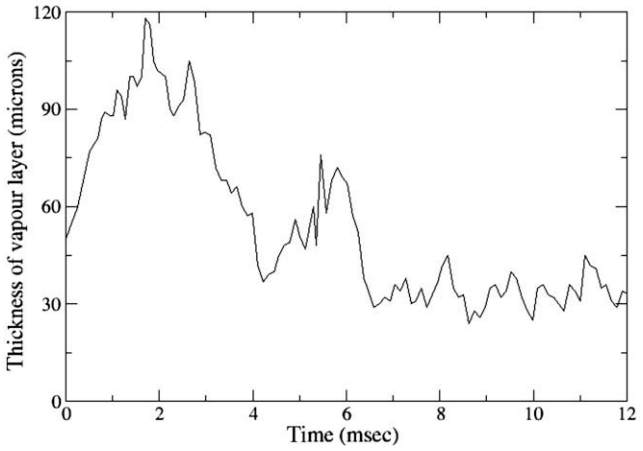

Fig. 2. Progress of the vapour layer thickness under the centre of the lower surface of a sessile droplet. Initially, the thickness exhibits oscillatory behaviour but eventually it settles between 20 and 40 μm.

rate based on local conditions, these observations suggest that the predicted behaviour would not be very different from that predicted by the average values implicit in the present uniform model.

Although it seems that the behaviour of a sessile droplet can be well-predicted, plainly the interaction of such droplets with walls does not involve phenomena as complex as those governing the dynamic 'impact' of a moving droplet. These are of course the circumstances of interest in the reflood process, and we now turn to a study of such cases.

4.3. Impacting droplet case

4.3.1. Experiment

For droplets that impact on a hot surface at a temperature exceeding the Leidenfrost temperature, there is no contact line (due to the presence of a thin interlayer of vapour below the droplet). The behaviour of these droplets was studied through experimental and analytical work by Biance et al. [3].

For droplets smaller than the capillary length, which for water at saturation temperature is approximately 2.5 mm, the most important parameter is the Weber number (We):

$$We = \frac{\rho U^2 R}{\sigma} \tag{15}$$

The experimental work of Biance et al. [3] focused mainly on filming millimetric droplets incident at various velocities. They investigated firstly the change of the droplet shape during the deformation, and then the dependence of the maximum droplet base radius on the impact velocity.

More specifically, in an initial experiment, a 1 mm radius water droplet was filmed during its interaction with a 300 °C hot steel plate (Fig. 3). The corresponding Weber number for this case was 10.

Then, by changing the height from which millimetric water droplets were released the impact velocities (and consequently the Weber number) were varied. It was demonstrated experimentally that for strong-deformation cases ($We > 1$) the maximum droplet base radius is a function of the Weber number, and an empirical correlation that fitted their experimental results was presented.

4.3.2. Analytical model

Biance et al. [3], also proposed a simple analytical model to predict maximum droplet base radius, built upon the earlier work of Chandra and Avedisian [37]. This earlier work was based on the theory that the kinetic energy converts to surface energy (the drop deforms as it hits the solid), and the Chandra and Avedisian [37] analysis concluded that this leads to the maximum radius scaling with Weber number to the power 1/2. The more recent analysis by [3] proposed that the dependence took the form

$$R_{\max} \propto RWe^{0.25} \tag{16}$$

where $R_{\max}$ is the maximum radius and R is the initial radius of the droplet. Biance et al. [3] demonstrated fairly good agreement of the experimentally obtained data with the analytical model they proposed. The observed maximum base radius scaled with Weber number to the power of 0.30 ± 0.005 instead of the 0.25 of the model.

4.3.3. Computational simulations

The initial two-dimensional axisymmetric simulation conducted here is of the millimetric water droplet studied experimentally by Biance et al. [3]. The density and viscosity ratios between the two phases are as for the sessile droplet case and $We = 11$ and $Re = 1367$. Evaporation is simulated with the mass transfer model described above, employing the same value of evaporation rate as for the sessile droplet.

In this case, the deformation processes are much more complex than in the sessile droplet case; the droplet hits the surface, spreads and then recoils due to surface tension forces.

A range of impact velocities was then examined for the same case. Direct comparison between the computational results and both the Biance et al. [3] analytical model and the Biance et al. [3] experimental data was made.

Deformation during the droplet–hot wall interaction. The computation employing TransAT© reproduces the shape of the droplet realistically. The computational results are compared in Fig. 3 with the series of pictures shown by Biance et al. [3].

During the initial period, as the droplet spreads, the height of the vapour layer at the centre exceeds that at the periphery of the droplet. Gradually, the thickness of the vapour layer becomes uniform over the base of the droplet. The droplet top gradually falls until it reaches a height significantly lower than the rim. The central part of the droplet starts doming up again and moving upwards. This procedure results in both the upper and the lower part of the droplet being lifted. The vapour layer acquires again a uniform thickness below the droplet. The droplet continues its upward motion and progressively gets longer and thinner.

The time for which the droplet is in close proximity to the surface is approximately 9 ms according to our simulation. This is in good agreement with the measured time of 11 ms by Biance et al. [3].

Dependence of the maximum radius of the droplet on the Weber number. In Fig. 4 we show a comparison of the measured results with the predictions of Biance's analytical model and the predictions of our simulation. Also shown is an empirical fit of our computed results.

At low Weber number the agreement is excellent. As the Weber number increases, the simulation seems to under-predict the experimental data; computed droplet maximum radii are slightly less than those observed. The results obtained by the simulation seem to match rather more closely the analytical model. The computed maximum radii scale with Weber number to the power of 0.23. This is close to the 0.25 of the analytical model. The experimental data scale with Weber number to the power of 0.30 ± 0.005.

5. Conclusions

Simulations of the interaction of evaporating droplets with hot surfaces have been made using the Level Set method embodied into the TransAT© code. We have investigated two cases: (i) a ses-

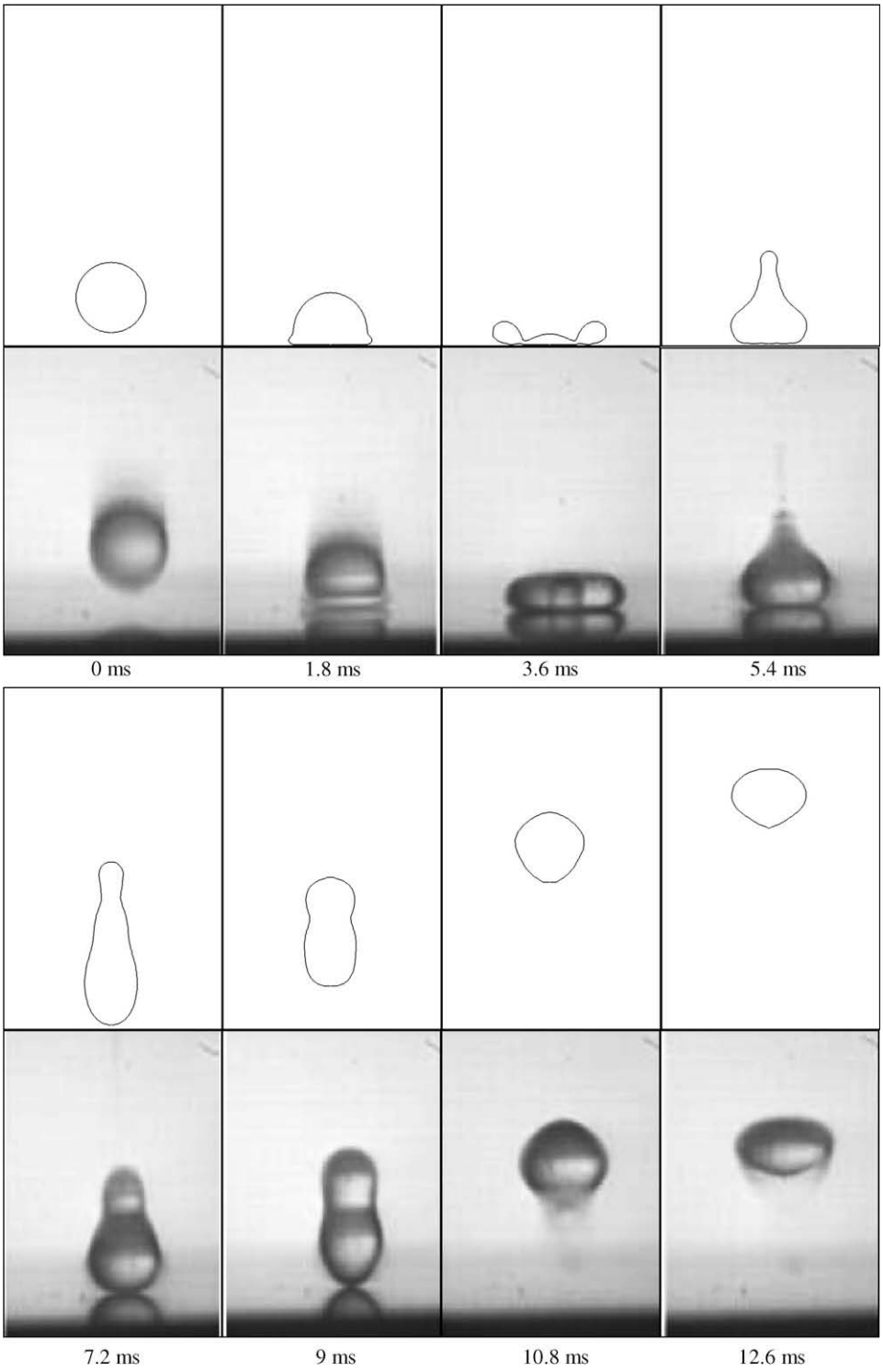

Fig. 3. Comparison between the two-dimensional axisymmetric simulation of a millimetric droplet impacting on a 300 °C solid surface ($We = 11$) and the experimental results of Biance et al. [3], ($We = 10$). The time interval between pictures is 1.8 ms.

sile drop, where we studied in particular the thickness of the vapour film, and (ii) an impacting drop, where we studied both the evolution of the droplet shape, and the maximum droplet radius attained during the interaction.

In both cases we obtain good qualitative and a large measure of quantitative agreement with measurement. For the sessile drop, evaporation rates and film thicknesses observed experimentally were well reproduced. For the impacting droplet, the observed vapour layer, droplet shape and hydrodynamic behaviour were also well reproduced.

This good agreement provides justification for the relatively simple uniform evaporation rate employed and provides a sound basis for extension to the mechanistic computation of heat removal from the hot surface during the interaction. This information will allow better understanding of the effect that the tiny saturated water droplets will have on the rod temperature during

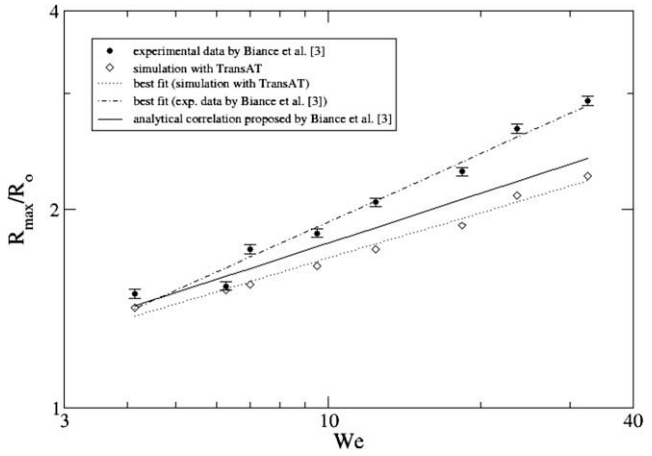

Fig. 4. The maximum radius (R_{max}) of an impacting water droplet as a function of *We* number. (Millimetric droplet, surface at 280 °C) Comparison between the present two-dimensional axisymmetric simulation and experimental results by Biance et al. [3]. The analytical correlation proposed by the same group of researchers is also plotted.

the reflood process as a result of their interaction with the hot fuel rods. Further development of the code is now being undertaken to allow direct mechanistic calculation of the evaporation rate based on local fluid conditions.

Acknowledgements

This work was carried out as part of the TSEC programme KNOO and as such we are grateful to the EPSRC for funding under Grant EP/C549465/1.

References

[1] J.G. Leidenfrost, De aquae communis nonnullis qualitatibus tractatus, Duisburgi ad Rhenum, Pars II (1756) 30–63.
[2] L.H.J. Wachters, H. Bonne, H.J. Van Nouhuis, The heat transfer from a horizontal plate to sessile water drops in the spheroidal state, Chemical Engineering Science 21 (1966) 923–936.
[3] A.-L. Biance, F. Checy, C. Clanet, G. Lagubeau, D. Quere, On the elasticity of an inertial liquid shock, Journal of Fluid Mechanics 554 (2006) 47–66.
[4] L.H.J. Wachters, N.A.J. Westerling, The heat transfer from a hot wall to impinging water droplets in the spheroidal state, Chemical Engineering Science 21 (1966) 1047–1056.
[5] A.-L. Biance, A.-L.C. Clanet, D. Quere, Leidenfrost drops, Physics of Fluids 15 (6) (2003) 1632–1637.
[6] C.O. Pedersen, An experimental study of the dynamic behaviour and heat transfer characteristics of water droplets impinging upon a heated surface, International Journal of Heat and Mass Transfer 13 (1970) 369–381.
[7] K. Okumura, F. Chevy, D. Richard, D. Quere, C. Clanet, Water spring: a model for bouncing drops, Europhysics Letters 62 (2) (2003) 237.
[8] F.H. Harlow, J.P. Shannon, The splash of a liquid droplet, Journal of Applied Physics 38 (1967) 3855.
[9] M. Bussmann, J. Mostaghimi, S. Chandra, On a three-dimensional volume tracking model of drop impact, Physics of Fluids 11 (1999) 1406–1417.
[10] M. Bussmann, S. Chandra, J. Mostaghimi, Modeling the splash of a droplet impacting a solid surface, Physics of Fluids 12 (2000) 3121–3132.
[11] D.B. Kothe, R.C. Mjolsness, Ripple: a new model for incompressible with free surfaces, AIAA Journal 30 (1992) 2694–2700.
[12] J.U. Brackbill, D.B. Kothe, C. Zemach, A continuum method for modelling surface tension, Journal of Computational Physics 100 (1992) 335.
[13] M. Pasandideh-Fard, R. Bhola, S. Chandra, J. Mostaghimi, Deposition of tin droplets on a steel plate: simulation and experiments, International Journal of Heat and Mass Transfer 41 (1998) 2929–2945.
[14] M. Pasandideh-Fard, S. Chandra, J. Mostaghimi, A three-dimensional model of droplet impact and solidification, International Journal of Heat and Mass Transfer 45 (2002) 2229–2242.
[15] H.C. Wu, W.S. Hwang, H.J. Lin, Development of a three-dimensional simulation system for micro-inkjet and its experimental verification, Materials Science and Engineering: A 373 (2004) 268–278.
[16] J. Fukai, Z. Zhao, D. Poulikakos, C.M. Megaridis, O. Miyatake, Modeling of the deformation of a liquid droplet impinging upon a flat surface, Physics of Fluids 5 (1993) 2588–2599.
[17] J. Fukai, Y. Shiiba, T. Yamamoto, O. Miyatake, Wetting effects on the spreading of a liquid droplet colliding with a flat surface: experiment and modelling, Physics of Fluids 7 (1995) 236–247.
[18] B. Perot, R. Nallapati, A moving unstructured staggered mesh method for the simulation of incompressible free-surface flows, Journal of Computational Physics 184 (2003) 192–214.
[19] T.A. Baer, R.A. Cairncross, P.R. Schunk, R.R. Rao, P.A. Sackinger, A finite element method for free surface flows of incompressible fluids in three dimensions. Part II: Dynamic wetting lines, International Journal of Numerical Methods in Fluids 33 (2000) 405–427.
[20] A. Theodorakakos, G. Bergeles, Simulation of sharp gas–liquid interface using VOF method and adaptive grid local refinement around the interface, International Journal of Numerical Methods in Fluids 45 (2004) 421–439.
[21] M. Francois, W. Shyy, Computations of drop dynamics with the immersed boundary method, part 2: drop impact and heat transfer, Numerical Heat Transfer Journal Part B 44 (2003) 119–143.
[22] N. Hatta, H. Fujimoto, H. Takuda, Deformation process of a water droplet impinging on a solid surface, ASME Transactions, Journal of Fluids Engineering 117 (1995) 394–401.
[23] H. Fujimoto, N. Hatta, Deformation and rebounding processes of a water droplet impinging on a flat surface above Leidenfrost temperature, ASME Transactions, Journal of Fluids Engineering 118 (1996) 142–149.
[24] H. Fujimoto, T. Ogino, H. Takuda, N. Hatta, Collision of a droplet with a hemispherical static droplet on a solid, International Journal of Multiphase Flow 27 (2001) 1227–1245.
[25] H. Fujimoto, I. Takezaki, Y. Shiotani, A.Y. Tong, H. Takuda, Collision dynamics of two droplets impinging successively onto a hot solid, ISIJ International 44 (2004) 1049–1056.
[26] D. Caviezel, C. Narayanan, D. Lakehal, Adherence and bouncing regime map of droplet impact on non-wetting surfaces, in: Sixth International Conference on Multiphase Flow, ICMF 2007, Leipzig, Germany, July 9–13, 2007 (S4 Wed D 42).
[27] D. Lakehal, M. Meier, M. Fulgosi, Interface tracking towards the direct simulation of heat and mass transfer in multiphase flows, International Journal of Heat and Fluid Flow 23 (2002) 242–257.
[28] D. Lakehal, G. Larrignon, C. Narayanan, Computational heat transfer and two-phase flow topology in miniature tubes, Microfluid Nanofluid, doi:10.1007/s10404-007-0176-1.
[29] A. Karl, K. Anders, M. Rieber, A. Frohn, Deformation of liquid droplets during collisions with hot walls: experimental and numerical results, Particle and Particle Systems Characterization 13 (1996) 186–191.
[30] D.J.E. Harvie, D.F. Fletcher, A hydrodynamic and thermodynamic simulation of droplet impacts on hot surface, Part I, theoretical model, International Journal of Heat and Mass Transfer 44 (2001) 2633–2642.
[31] D.J.E. Harvie, D.F. Fletcher, A hydrodynamic and thermodynamic simulation of droplet impacts on hot surface, Part II, validation and applications, International Journal of Heat and Mass Transfer 44 (2001) 2643–2649.
[32] Y. Ge, L.S. Fan, Three-dimensional simulation of impingement of a liquid droplet on a flat surface in the Leidenfrost regime, Physics of Fluids 17 (2005) (Art. No. 127104).
[33] Y. Ge, L.S. Fan, 3D modeling of the dynamics and heat transfer characteristics of subcooled droplet impact on a surface with film boiling, International Journal of Heat and Mass Transfer 49 (2006) 4231–4249.
[34] J.C. Chen, K.K. Hsu, Heat transfer during liquid contact on superheated surfaces, ASME, Journal of Heat Transfer 117 (1995) 693–697.
[35] S.J. Osher, J.A. Sethian, Fronts propagating with curvature dependent speed: algorithms based on Hamilton–Jacobi formulations, Journal of Computational Physics 79 (1988) 12–49.
[36] M. Sussman, P. Smereka, S. Osher, A level set approach for computing solutions to incompressible two-phase flow, Journal of Computational Physics 114 (1) (1994) 114–146.
[37] S. Chandra, C.T. Avedisian, On the collision of a droplet with a solid surface, Proceedings of the Mathematical and Physical Science 432 (884) (1991) 13–41.